International Journal of Engineering Research & Technology (IJERT)
ISSN: 2278-0181
Vol. 1 Issue 8, October - 2012

Performance Improvement Of A Louver-Finned Automobile Radiator Using Conjugate Thermal CFD Analysis

Junjanna G.C
Team Leader
Ford Technology Services India,
Chennai, India.

Dr. N Kulasekharan
Professor & Head
Department of Mechanical Engineering
Saveetha Engineering College, Chennai
Tamil Nadu, India.

Dr. H.R. Purushotham
Associate Professor
Department of Mechanical Engineering
Siddaganga Institute of Technology, Tumkur, India

Abstract

Radiators are used to transfer thermal energy from one medium to another for the purpose of cooling. Research is being carried out for several decades now, in improving the performance of the heat exchangers, having high degree of surface compactness and higher heat transfer abilities in automotive industry. These compact heat exchangers have fins, louvers and tubes.

Present study uses the computational analysis tool ANSYS Fluent 13.0 to perform a numerical study on a compact heat exchanger. The computational domain is identified from literature and validation of present numerical approach is established first. Later the numerical analysis is extended by modifying chosen geometrical and flow parameters like louver pitch, air flow rate, water flow rate, fin and louver thickness, by varying one parameter at a time and the results are compared. Recommendations has been made on the optimal values and settings based on the variables tested, for the chosen compact heat exchanger.

1. Introduction

Radiators are heat exchangers used to transfer thermal energy from one medium to another for the purpose of cooling. Radiators are used for cooling internal combustion engines, mainly in automobiles but also in piston-engine aircraft, railway locomotives, motorcycles, stationary generating plant. The radiator transfers the heat from the fluid inside to the air outside, thereby cooling the fluid, which in turn cools the engine. Figure 1 shows a typical radiator used in automobile.

Radiators are also often used to cool automatic transmission fluids, air conditioner refrigerant, intake air, and sometimes to cool motor oil or power steering fluid. Radiators are typically mounted in a position where they receive airflow from the forward movement of the vehicle, such as behind a front grill.

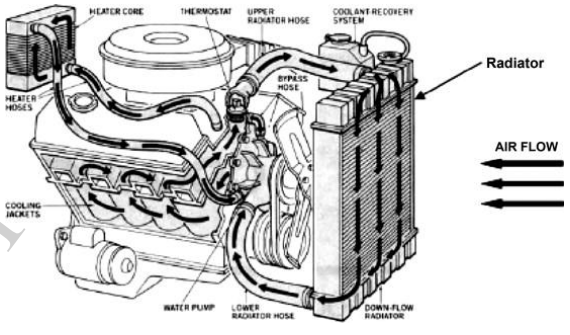

Fig. 1 A typical automobile radiator [1]

Where engines are mid- or rear-mounted, it is common to mount the radiator behind a front grill to achieve sufficient airflow, even though this requires long coolant pipes. Alternatively, the radiator may draw air from the flow over the top of the vehicle or from a side-mounted grill. For long vehicles, such as buses, side airflow is most common for engine and transmission cooling and top airflow most common for air conditioner cooling. Radiators used in automotive applications fall under the category of compact heat exchangers.

For the purposes of the ECA (Enhanced Capital Allowance) Scheme, a CHE is defined as a heat exchanger with a surface to volume ratio of more than 200 m^2/m^3. There are two primary classifications of heat exchangers according to their flow arrangement, parallel flow and counter flow. In parallel-flow heat exchangers, the two fluids enter the exchanger at the same end, and travel in parallel to one another to the other side. In counter-flow heat exchangers the fluids enter the exchanger from opposite ends.

The counter current design is the most efficient, in that it can transfer the most heat from the heat (transfer) medium due to the fact that the average temperature difference along any unit length is greater. For efficiency, heat exchangers are designed to maximize the surface area of the wall between the two fluids, while minimizing resistance to fluid flow through the exchanger. The exchanger's performance can also be affected by the addition of fins or corrugations in one or both directions, which increase surface area and may channel fluid flow or induce turbulence.

A heat exchanger is a piece of equipment built for efficient heat transfer from one medium to another. The media may be separated by a solid wall, so that they never mix, or they may be in direct contact. The classic example of a heat exchanger is found in an internal combustion engine in which a circulating fluid known as engine coolant flows through radiator coils and air flows past the coils, which cools the coolant and heats the incoming air.

Borrajo-Pelaez *et. al.* [2] carried out 3D numerical simulations to compare both an air side and air/water side model of a plain fin and tube heat exchanger. In their experiment, the influence of the Reynolds number, fin pitch, tube diameter, and fin length and fin thickness were studied. Haci Mehmet Sahin *et. al.* [3] studied the heat transfer and pressure drop characteristics of seven different fin angles with plain fin and tube heat exchangers. This problem was analyzed using fluent software, and it was found that a fin with 30º inclination is the optimum one, which gives the maximum heat transfer enhancement. Mao-Yu Wen *et. al.* [4] have investigated the heat transfer performance of a fin and tube heat exchanger with three different fin configurations such as plate fin, wavy fin and compounded fin. This experiment strongly suggested the use of the compound fin configuration for the heat exchanger.

Wei-Mon Yan and Pay-Jen Sheen [5] have carried out an experiment to investigate the heat transfer and pressure drop characteristics of fin and tube heat exchangers with plate, wavy and louvered fin surfaces. From this experiment, it is found that at the same Reynolds number, louvered fin geometry shows larger values of *f* (friction) and *j* (colburn) factors, compared with the plate fin surfaces. Igor Wolf *et. al.* [6] studied the heat transfer performance of a wavy fin and tube heat exchanger by numerical and experimental methods. They presented the results of a three dimensional numerical analysis of heat transfer on the air side of a wavy fin and tube heat exchanger. The three dimensional local flow and thermal fields are well characterized by the numerical analysis. The developed and presented model demonstrated good heat transfer prediction. It could provide guidelines for the design optimization of a fin and tube heat exchanger. In this study, three rows of circular tubes in a staggered arrangement were taken as a domain. The air-side heat transfer and pressure drop characteristics were successfully modelled using the CFD software Fluent. The numerical results were validated with the experimental results and the deviation was within 8%.

Tang *et. al.* [7] carried out an experimental and numerical investigation on the air-side performance of fin and tube heat exchangers with various fin patterns, such as crimped spiral fin, plain fin, slit fin, fin with delta wing longitudinal vortex generator (VG), and mixed fin with front 6-row vortex generator fin and rear 6-row slit fin. It was found that the heat exchanger with the crimped spiral fin has better performance than the other four configurations. Also it is found that the Slit fin offers the best heat transfer performance at a higher Reynolds number. Wang *et. al.* [8] provided flow visualization and pressure drop results for plain fin and tube heat exchangers, with and without the presence of vortex generators. It was found that the pressure drop of the delta winglet is lower than that of the annular winglet.

Fiebig *et. al.* [9] investigated the local heat transfer and flow losses in plate fin and tube heat exchangers with vortex generators, to compare the performance of round and flat tubes. It was found that the heat exchanger with flat tubes and vortex generators gives nearly twice as much heat transfer with a penalty of 50% pressure loss, when compared to a heat exchanger with round tubes. Leu *et. al.* [10] had performed a numerical and experimental analysis to study the thermo-hydraulic performance of an inclined block shape vortex generator embedded plate fin and tube heat exchangers. In this analysis, the effects of different span angles (30º, 45º and 60º) were investigated for Reynolds numbers ranging from 400 to 3000. It was found that a 30º span angle provides the best heat transfer augmentation and also offers 25% lesser fin surface area. Leu *et. al.* [11] conducted a numerical simulation for louvered fin and tube heat exchangers having circular and oval tube configurations. The effects of the geometrical parameters such as louver angle, louver pitches and louver length were discussed.

Joen *et. al.* [12] worked on the interaction between the flow behavior (flow deflection and transition to unsteady flow) and the thermo-hydraulic performance of an inclined louvered fin design. In this experiment, the impact of fin pitch, fin angle and Reynolds number were discussed in detail. Zhang and Tafti [13] investigated the effect of the Reynolds number, fin pitch, louver thickness and louver angle on flow efficiency in multi-louvered fins and found that the flow efficiency (flow efficiency (η) = Mean flow angle (αmean) / Louver angle (θ)) is strongly dependent on geometrical parameters, especially at a low

Reynolds number. The Flow efficiency increases with the Reynolds number and louver angle, while decreasing with the fin pitch and thickness ratio.

Wei Li and Xialing Wang [14] conducted an experimental study on the air side heat transfer and pressure drop characteristics of brazed aluminium heat exchangers, with multi-region louver fins and flat tubes. They found that the heat transfer coefficients and pressure drop tend to decrease with increasing Reynolds numbers, and increase with the number of louvers. Wang *et. al.* [15] presented generalized heat transfer and friction correlations for louver fin geometry having a round tube configuration. They considered different geometrical parameters, such as louver pitch, louver height, longitudinal tube pitch, transverse tube pitch, tube diameter and fin pitch for the generation of correlations.

The literature survey discussed so far shows that large number of literature is available both experimental and numerical analysis of radiator. Present work deals with the radiator as applied to automotive industry which is a form of compact heat exchanger with alternate layers of fin and tubes, as shown in Fig. 2. Depending on the application, various fin patterns such as plate, louver, convex-louver and wavy are used in the fin side (air side). They have a high degree of surface compactness and substantial heat transfer enhancement, obtained as a result of the periodic starting and development of the laminar boundary layers, over interrupted channels formed by the fins and their dissipation in the fin wakes.

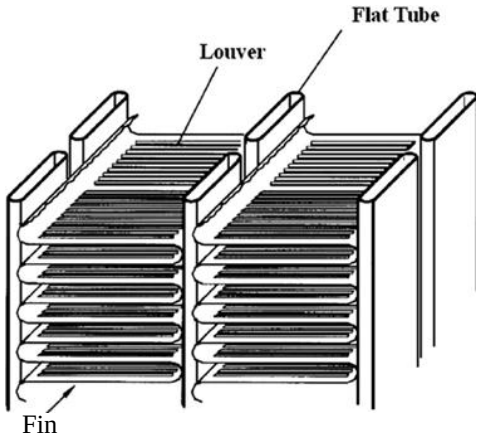

Fig. 2 Water tube, fin and louver in a typical automotive radiator [16]

Figure 3 shows the louver arrangement in a fin used in an automotive radiator. Although lot of work has been done so far in the computational analysis for the compact heat exchangers, validation of an experimentally tested domain and conducting analysis of modified designs to optimize the design and improve performance on the same domain was not reported so far. This forms the motivation of the present work.

Thus, the objective of the present work is to identify an experimental work from literature, perform computational analysis for the domain studied experimentally to validate the present numerical work. The second objective is to perform geometrical and flow parameter study on the domain identified by varying louver pitch, air flow rate, water flow rate, fin and louver thickness, one parameter at a time. Comparison of these numerical results will help in identifying the optimal combination of geometrical and flow parameters for the domain selected.

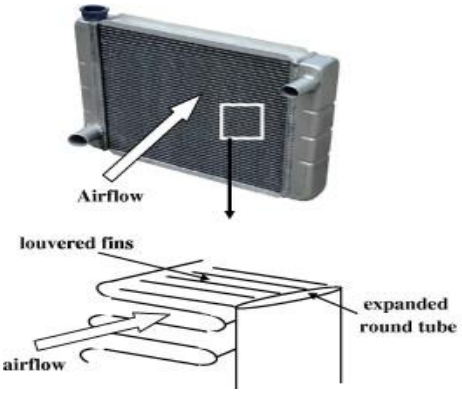

Fig. 3 Fins and louver in a typical radiator [17]

2. Brief description of Experimental Work [16]

The experimental work identified from the open literature to validate the present computational methodology is that of Vaishi *et. al.*, and will be discussed in detail in this chapter. In this study [16], the authors tested air-side heat transfer and pressure drop characteristics of flow over louvered fins in compact heat exchangers experimentally. The test samples consist of two types of fin configurations. A series of tests were conducted to examine the geometrical parameters of louver pitch, louver arrangement (symmetrical and asymmetrical) and number of louver regions.

Their calculated results indicate that a symmetrical arrangement of louvered fins provides a 9.3% increase in heat transfer performance and a 18.2% decrease in pressure drop than the asymmetrical arrangement of louvered fin. Also, for a constant rate of heat transfer and pressure drop, a 17.6% decrease of fin weight is observed for the symmetrical arrangement of fins and this is following by considerable decrease in total weight and cost of the heat exchanger. The results from this investigation indicate that the configuration of the louvered fins has the dominant influence on the heat transfer and pressure drop.

3. Physical model

Figure 4 shows the geometric construction details of the louvered, finned compact heat exchanger [16] studied presently. The louver with a symmetry pattern domain is chosen for the present

numerical study. The fin geometry indicates that it has a periodicity in the tube height-wise (span) direction and in the lateral direction too.

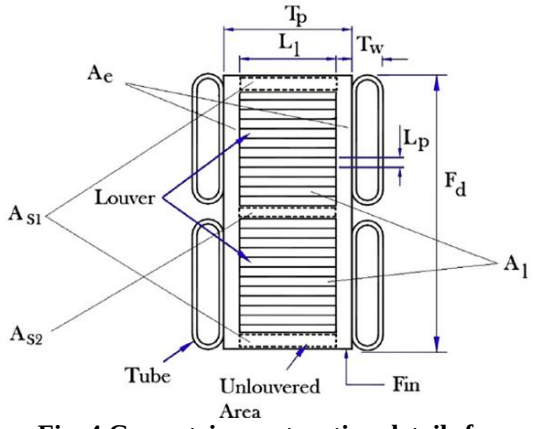

Fig. 4 Geometric construction details from Vaisi et al [16]

Due to the symmetry of the geometry, the computational domain is confined to one fin pitch in the span-wise direction and one tube pitch in the lateral direction, which is highlighted with a dashed red line. Since the geometry of the heat exchanger is periodic in nature, a smaller portion of the geometry is considered for the computational analysis, as shown in Fig. 5

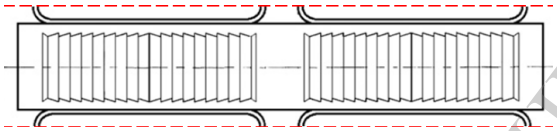

Fig. 5 Periodic computational domain identified

The length, breadth and height of the computational domain are 64mm, 10.5mm (tube pitch) and 2.7mm (fin pitch) respectively. To minimize the error due to flow oscillations and flow reversing effects, which might get induced numerically, the computational domain is extended in the stream-wise direction of air. Additional air domain considered upstream and downstream of the heat exchanger helps to avoid un-realistic recirculation zones in the domain. Louver geometric details are shown in Fig.6 and a close view of the fin shape is shown in Figs.7.

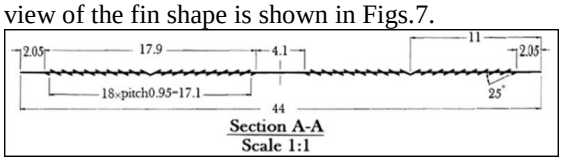

Fig. 6 Louver geometry dimensions as tested by Vaisi *et al* [16]

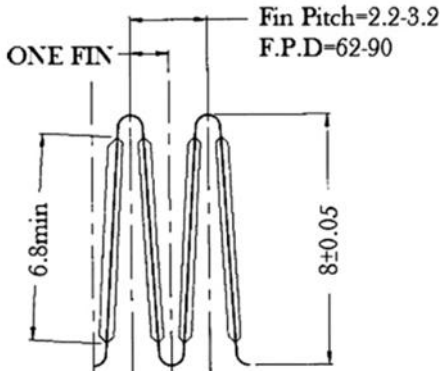

Fig. 7 Details of fin shape as tested by Vaisi *et al* [16]

4. Mathematical model

The CFD software Fluent is employed for simulation. In the Fluent, the conservation equations of the mass, momentum and energy are solved using the finite volume method. The Reynolds transport equations are written in a generalized form (H.K. Versteeg and W. Malalasekera [17]).

$$div\,(\rho u\varphi) = div\,(\Gamma\, grad\,\varphi) + S \qquad (1)$$

where φ stands for a generalized transport variable, which is used for all conserved variables in a fluid flow problem, including, mass, momentum and the turbulence variables κ and ω. Γ represents the effective diffusivity (sum of the eddy diffusivity and the molecular diffusivity). S is the source term for the respective dependent variable.

The governing equations are as follows:

Mass conservation:

$$\nabla . (\rho\vec{v}) = 0 \qquad (2)$$

Momentum conservation:

$$\nabla.(\rho\vec{v}\vec{v}) = -\nabla p + \nabla.(\bar{\bar{\tau}}) \qquad (3)$$

Energy conservation:

$$\nabla_{\cdot}\left(\vec{v}\left(\rho E + p\right)\right) = \nabla\, k_{eff}\nabla T \qquad (4)$$

The assumptions made in the CFD simulation are that (a) the flow is stable in the computational domain with respect to time and (b) the fluid in the domain is incompressible. The solution of the above set of equations is obtained for the prediction of pressure, velocity and temperature throughout the domain. The computational domain is extended both upstream and downstream of the core, and the potential back flow is avoided.

The fundamental governing equations for flow and heat transfer of flow past multiple rows of cylindrical arrays are the continuity, momentum (Navier-Stokes) and energy equations along with the equations for modeling the turbulence quantities. The assumptions made in formulating

these equations for the present investigations are: (1) flow is steady, (2) flow is incompressible, (3) there is no viscous dissipation, (4) constant material properties and (5) there are no buoyancy effects.

5. Turbulence closure

There are many options available within the solver in providing the turbulence closure using the RANS approach: (i) zero equation (algebraic) models, (ii) half-equation models, (iii) one equation models, (iv) two-equation models, (v) second order models (Reynolds Stress Model) and (vi) algebraic stress models. Among the many turbulence models available, the widely used two equation models are *k-ε* and *k-ω*. These models provide computation of turbulence kinetic energy (*k*) and turbulence length scale or its equivalents. These eddy-viscosity methods are based on similarity reasoning that turbulence is a physical concept connected to the viscosity.

The simplest "complete models" of turbulence are two-equation models in which the solution of two separate transport equations allows the turbulent velocity and length scales to be independently determined. The standard k-ε model in Fluent® falls within this class of turbulence model and has become the workhorse of practical engineering flow calculations in the time since it was proposed by Launder and Spalding [18]. Robustness, economy, and reasonable accuracy for a wide range of turbulent flows explain its popularity in industrial flow and heat transfer simulations. It is a semi-empirical model, and the derivation of the model equations relies on phenomenological considerations and empiricism.

The realizable *k-ε* model developed by Shih *et. al.* [19] is a relatively recent development and differs from the standard *k-ε* model in two important ways. The realizable *k-ε* model contains a new formulation for the turbulent viscosity. A new transport equation for the dissipation rate, ε, has been derived from an exact equation for the transport of the mean-square vorticity fluctuation. The term "realizable" means that the model satisfies certain mathematical constraints on the Reynolds stresses, consistent with the physics of turbulent flows. Neither the standard k-ε model nor the RNG *k-ε* model is realizable.

An immediate benefit of the realizable k-ε model is that it more accurately predicts the spreading rate of both planar and round jets. It is also likely to provide superior performance for flows involving rotation, boundary layers under strong adverse pressure gradients, separation, and recirculation. The standard *k-ω* model in Fluent® is based on the Wilcox [20] model, which incorporates modifications for low-Reynolds-number effects, compressibility, and shear flow spreading. The Wilcox model predicts free shear flow spreading rates that are in close agreement with measurements for far wakes, mixing layers, and plane, round, and radial jets, and is thus applicable to wall-bounded flows and free shear flows. The standard *k-ω* model is an empirical model based on model transport equations for the turbulence kinetic energy (*k*) and the specific dissipation rate (*ω*), which can also be thought of as the ratio of *ε* to *k*.

A suitable turbulence model to be used for the present simulations which is identified from the literature is the *k-ω* model available within the solver. This may be attributed to the ability of the turbulence model to capture large fluid strains more accurately.

6. CFD Approach

The finite volume based Computational Fluid Dynamics (CFD) technique is used to predict the flow and heat transfer aspects in a cross flow heat exchanger, used in a automobile application. Simulations are carried out for heat exchanger models with different louver pitches, air and water flow rates and at different fin, louver thicknesses. Analysis of heat exchanger with fins and louvers were conducted. Parameters like louver shape is modified to study their influence on overall heat exchanger effectiveness.

Gambit 2.4.3® software is used as the pre-processor tool to model the computational domains. The commercial CFD code Fluent 13.0 is used for simulations in the present conjugate heat transfer analysis. Continuity, momentum and energy equations for a three dimensional, incompressible flows are solved on the double periodic domain. The code uses a pressure correction based finite volume solver. Fluid domain is air which cross flows over the water tubes and the solid domain modeled to effect conjugate heat transfer.

The CFD approach for both the pressure drop and the heat transfer prediction across the test unit is explained in this section. In the present numerical simulations air (ρ = 1.225 [kg m^{-3}], μ = 1.7894 x 10^{-05} [kg $m^{-1}s^{-1}$], C_p = 1.006 [kJ $kg^{-1}K^{-1}$] and Pr = 0.706) is used as the working fluid in the fin side and water (ρ = 998.2 [kg m^{-3}], μ = 0.001003 [kg $m^{-1}s^{-1}$], C_p = 4.182 [kJ $kg^{-1}K^{-1}$] and Pr = 0.7) is used as the working fluid in the tube side.

7. Boundary conditions

The analysis being carried out in conjugate mode, conduction and convection parameters are estimated by the solver based on local flow and thermal conditions. Air, water entry flow and thermal conditions are specified as boundary conditions for the computations. All internal flow and thermal conditions are calculated in a conjugate manner. Thus the fin, louver and tube surface heat transfer rates all are calculated and not specified as boundary condition. The local and averaged heat transfer coefficient values on the

wall surfaces are estimated based on thermal and flow turbulence calculations by the solver. The boundary conditions used for the present validation CFD analysis where both hot water and cold air make cross flow in the domain are discussed below (for the validation case using the baseline model):

Air Inlet :

Calculated velocity equivalent to the flow rates used in the experiments were used at the inlet.

The flow is assumed to enter normal to the inlet boundary surface and assumed to enter uniformly.

- Inlet velocity: 9.71m/s
- Inlet temperature: 20.3^{o}C
- Outlet temperature: 300 K (applicable only to the grid cells with back flow)

Water inlet:

From the total water flow rate specified in the literature, the flow rate per tube is calculated and used in the analysis. Water flows inside the tube in a direction normal to the air flow direction.

- Inlet flow rate: 120 LPM
- Inlet temperature: 80^{o}C
- Outlet temperature: 80^{o}C (applicable only to the grid cells with back flow)

Outlet:

Normal to the boundary surface and assumed exiting at 'zero' static pressure.

Wall surfaces:

Walls are assumed smooth and without slip.

- u=0, v=0 and w =0
- No separate thermal boundary condition needed, as the solver calculates the thermal information in a coupled way.

Left, right sides and upper, lower sides of the domain are declared periodic because of the geometrical periodicity.

- Across the left, right periodic faces: $\partial\varphi/\partial x=0$
- Across the upper, lower faces: $\partial\varphi/\partial y=0$

Since the tube, fin and louver walls are very thin compared to the overall dimension of the computational domain, they are modeled as thin surfaces and wall thickness is added virtually in the solver. This is done in order to decrease the overall computational mesh size, which will eventually help in decreased computational time. The boundary surfaces used in the numerical analysis are marked in Fig.8.

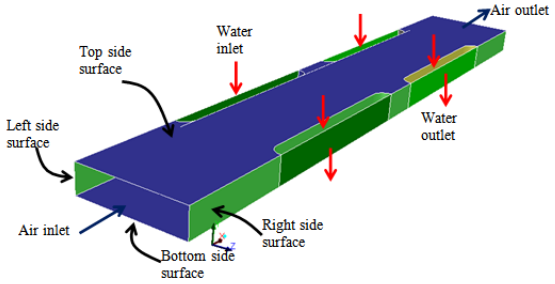

Fig. 8. Boundary surfaces as used in the numerical analysis

The properties of materials used for the present numerical study is taken from the Fluent solver material database itself. The operating pressure is atmospheric with 101.325 kPa absolute pressure and gravity is not considered as the influence of buoyancy is assumed minimal in this case.

8. Initial condition

The radiator is assumed to have reached steady state or equilibrium condition, for the chosen combination of water, air temperature and flow rates. Hence steady state conjugate thermal CFD analysis were carried out presently. Flow is assumed incompressible in both air and water sides.

9. Computational methodology

SIMPLE scheme is used to couple the pressure and velocity equations to derive the pressure correction equation. Second order up-winding scheme is used to have higher order accuracy. The homogeneous method of conjugate heat transfer (combined mode of conduction and convection) is employed by Fluent® which facilitates direct coupling of fluid zone and solid zone using the same discretization and numerical approach. Hence it is possible to have an interpolation-free crossing of the heat fluxes between the neighbouring cell faces.

The solver parameters are steady, implicit, absolute velocity formulation with Green-Gauss cell based gradient options. The flow is assumed turbulent and incompressible and the channel exit is open to atmosphere. The scaled residuals for the solution convergence are set to 10^{-5} for all governing equations, turbulence quantities whereas it was set as $10e^{-7}$ for energy and once met, the solution is considered to be converged. For a few turbulence model studies, when the convergence is not achieved to the desired accuracy, the iteration is continued further to a stage that the results do not vary even after 500 iterations, thus achieving iterative convergence.

10. Grid Independency Study

Tetrahedral mesh elements are used for meshing the computational model. Surface mesh element sizes are controlled to obtain fine mesh elements close to fin and louvers. Mesh grows in size outward from the fin, louver to the tubes and extended domains.

Analysis was carried out initially to study the influence of grid density on the computational results on the baseline case. Temperature along a horizontal line is considered as the criteria for grid independency and the variation of temperature along the line is plotted in Fig. 9 Surface mesh size range from 0.2 to 0.4. Different mesh sizes, starting with very coarse to very fine mesh are considered and analyzed at a particular Reynolds number. Three different grids were tested with 1.0, 1.5 and

2.5 million cells. The k-ω turbulence model is used for the present numerical simulations.

Figure 9 shows the air temperature variation along the length of the channel. Channel with a grid density of 1 Million cells shows lower temperatures compared to other two grid densities. Lesser variation is observed between domains with 1.5Mi and 2.5Mi cells. Hence a grid density of 1.5 million cells was chosen to continue with the analysis.

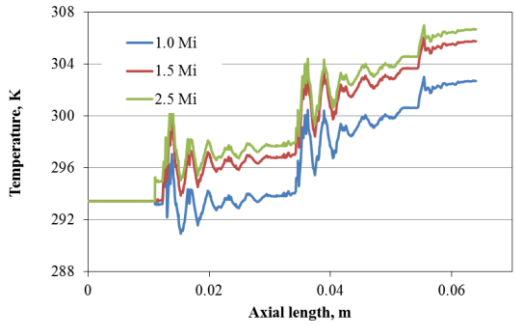

Fig. 9 Axial air temperature variation along the length of the channel

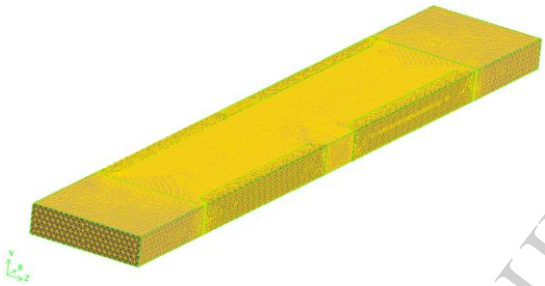

Fig. 10 Meshed computational domain

Further study of other flow parameter and geometry variation studies are carried out using this mesh density. The meshed computational domain is shown in Fig. 10, with the chosen mesh size of 1.5 million cells.

Initially computations are performed for the baseline model with the chosen mesh size and density and the results are compared with that of the experiments of Vaisi *et al* [16]. Further to the validation of the presently adopted computational methodology, the numerical analysis is extended to study including some geometrical and flow variations. Few geometric parameters are fixed and few parameters are varied.

The Fixed parameters are:

- Fin geometry: Corrugated;
- Fin pitch: 2.7 mm
- Louver angle: 25 deg.
- Tube pitch: 10.5mm
- Air inlet temperature: 20.3 deg C
- Water inlet temperature: 80 deg C

A summary of the cases solved in the present study are detailed in Table 1 and the parameters which were varied are highlighted. It is to be noted that the Case-01 forms the baseline case which represents the case as tested by Vaisi *et al* [16].

Table 1. Summary of cases solved presently

	Louver pitch	Air velocity	Water flow	Fin thk	Louver thk
Effect of Louver Pirch					
	mm	m/s	LPM	mm	mm
Case-01	0.95	9.71	120	0.08	0.08
Case-02	1.43	9.71	120	0.08	0.08
Case-03	1.90	9.71	120	0.08	0.08
Case-04	2.38	9.71	120	0.08	0.08
Case-05	2.85	9.71	120	0.08	0.08
Effect of air flow rate					
	Louver pitch	Air velocity	Water flow	Fin thk	Louver thk
	mm	m/s	LPM	mm	mm
Case-06	0.95	5.58	120	0.08	0.08
Case-07	0.95	6.81	120	0.08	0.08
Case-08	0.95	8.09	120	0.08	0.08
Case-09	0.95	10.64	120	0.08	0.08
Case-10	0.95	11.9	120	0.08	0.08
Effect of water flow rate					
	Louver pitch	Air velocity	Water flow	Fin thk	Louver thk
	mm	m/s	LPM	mm	mm
Case-11	0.95	9.71	80	0.08	0.08
Case-12	0.95	9.71	90	0.08	0.08
Case-13	0.95	9.71	100	0.08	0.08
Case-14	0.95	9.71	110	0.08	0.08
Case-15	0.95	9.71	130	0.08	0.08
Effect of fin, louver thickness					
	Louver pitch	Air velocity	Water flow	Fin thk	Louver thk
	mm	m/s	LPM	mm	mm
Case-16	0.95	9.71	120	0.04	0.04
Case-17	0.95	9.71	120	0.12	0.12
Case-18	0.95	9.71	120	0.16	0.16
Case-19	0.95	9.71	120	0.2	0.2

11. Results and Discussions

Validation case (Case-01)

For the validation case, first the results from the experiments and the present computational work were compared to make sure that the present computational methodology is valid. Further to that the contours of flow and thermal properties on chosen locations are plotted. Contours and plots are extracted from the computational analysis and reported, which will give good insight into the flow and heat transfer physics.

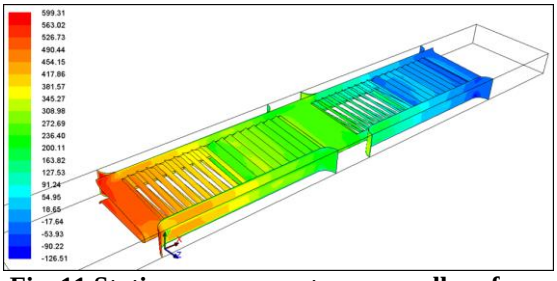

Fig. 11 Static pressure contour on wall surfaces – air side

Figure 11 shows the contours of air side pressure distribution on channel walls. Since the air

side inlet boundary condition is specified with a known value (say. 9.71m/s) and the channel outlet is assumed exhausting into atmosphere ie., a zero static pressure value, the solver adjusts the inlet pressure to maintain continuity across the channel.

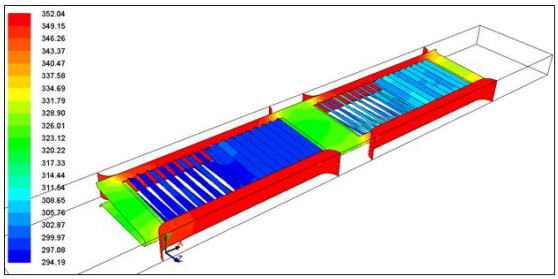

Fig. 12 Temperature contour on wall surfaces – air side (Case-01)

Figure 12 shows the contours of temperature on the wall surfaces of the computational domain considered. Water being hot, when passing through the water tubes heats them to reach higher temperature and by convection and conduction, heat gets transferred to the fins, louvers. Air cools the louvers and fins, by carrying the convection heat. Hence air temperature increases in the stream wise direction. Locations '1', '2' and '3' have more fin surface area than the regions with louvers. Heat transfer from hot water by conduction is more in these regions and hence higher fin surface temperatures are observed in these regions.

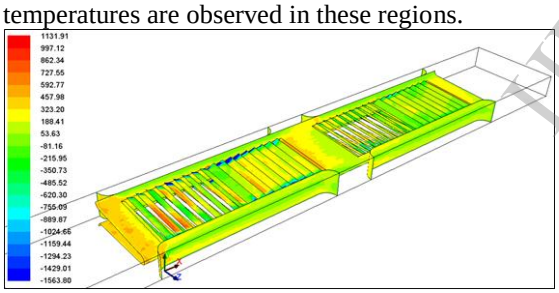

Fig. 13 Air side heat transfer coefficient contour on wall surfaces (Case-01)

Figure 13 shows the air side surface heat transfer coefficient on the wall surfaces. Higher heat transfer coefficient values are observed at the channel inlet and lower values are observed near the ends of the louvers due to local air recirculation is observed in these regions.

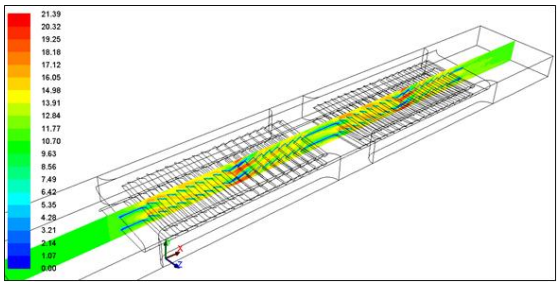

Fig. 14 Contours of velocity magnitude on a mid-vertical plane

Figure 14 shows the contours of velocity magnitude on a vertical plane passing through the air side stream wise direction and parallel to the water side stream wise direction. Velocity increases in the gap between the louvers. The louvers were found to deflect the air, thereby increasing the heat transfer by the way of increased turbulence levels downstream in the air stream.

Table 2 shows the comparison between the experimental data of Vaishi et al [16] and the results from the present CFD computations.

Table 2. Comparison of data between experiments of Vaisi *et al*. [16] and present CFD

Parameters		Expt.	CFD
Input boundary conditions			
Water inlet temperature	K	353.14	353.14
Air inlet temperature	K	293.44	293.44
Mass flow rate of air	kg/s	-	0.000337
CFD Estimated values			
Outlet water temperature	K	345.38	348.20
Outlet air temperature	K	318.84	312.16
Heat carried by air	W	-	6.42
Heat transfer rate	kW	56.28	80.94
Air side pressure drop	m.bar	6.40	5.41

The energy transfer in present computation showed higher heat transfer to the air, as compared to that in the experiments. This can be attributed to the fact that the present computations do not considered the heat loss from the radiator to the ambient, where this loss will be predominant in the experiments. Overall, the table shows good agreement between the experimental data and present numerical results. Thus the present computational methodology is vindicated.

Effect of Louver Pitch (Cases 01-05)

Five louver pitch variations are studied presently viz., 1.43mm, 1.90mm, 2.38mm, and 2.85mm (in addition to the baseline louver pitch value of 0.95mm) which are identified presently as Case-02 to Case-05 respectively. Case-01 being the baseline case, the results from this case was analyzed in detail when validating the computational methodology earlier here. Hence, the results from the other four cases Case-02 to Case-05 are discussed below.

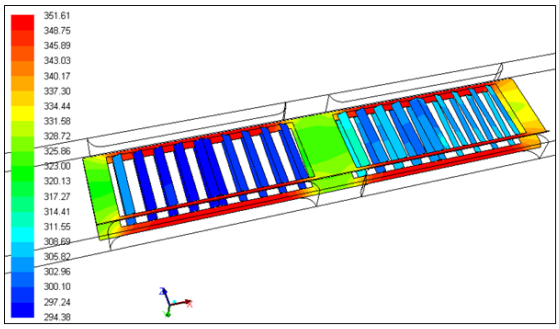

Fig. 15 Air side heat transfer coefficient contour on wall surfaces (case-03).

Figure 15 shows the distribution of surface heat transfer coefficient 'h' on the channel walls. Higher values of heat transfer coefficient were observed in the fin facing the air (ahead of the first row tube). Louvers immediate downstream showed lower values of 'h' since the heat transferred from the fins to the louvers are small due to lower contact area. Louvers in the second tube row showed higher 'h' values than the louvers in the first tube row area.

Further increase in louver pitch would result in poor number of louver availability in the domain, thus creating large openings in the fin. Fig. 16 compares the effect of louver pitch variation on the water outlet temperature. With increasing the louver pitch, not much influence is observed in the water outlet temperature. This water temperature is estimated by averaging all four half tube outlets. The variation is in the second decimal and hence negligible.

Figure 17 shows the air side heat transfer coefficient variation with increased louver pitch. For a louver pitch of 1.9mm the value of heat transfer coefficient come down and increases again.

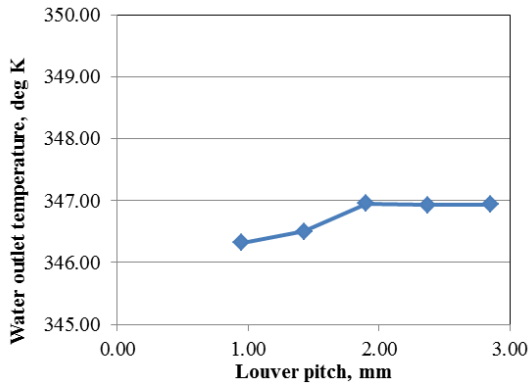

Fig. 16 Effect of louver pitch variation on water outlet temperature

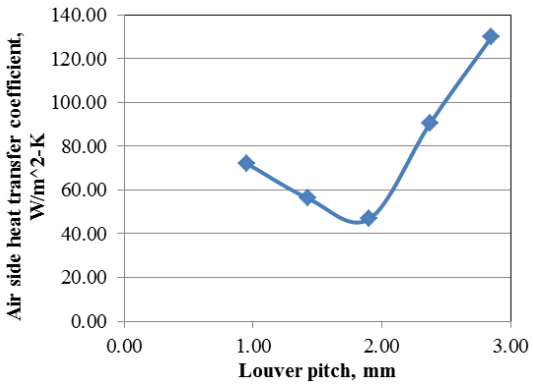

Fig. 17 Effect of louver pitch variation on air side heat transfer coefficient

Effect of Air Flow Rate (Cases 06-10)

Air flow rate is varied from 5.58 (Case-06) to 11.9m/s (Case-10) as tested experimentally by Vaishi *et al* [16]. The results are reported here for the lowest and highest air velocity to understand the influence of this parameter on the flow and heat transfer characteristics of the channel.

Figure 18 shows the heat transfer coefficient contours on the wall surfaces (Case-06). Louvers showed lower wall surface heat transfer coefficients 'h' compared to the fin regions. Louvers in the first tube row region shows lower 'h' values than its counterparts near the second row tube. Fin surface close to the water tubes showed highest heat transfer coefficient indicating higher heat transfer through these surfaces.

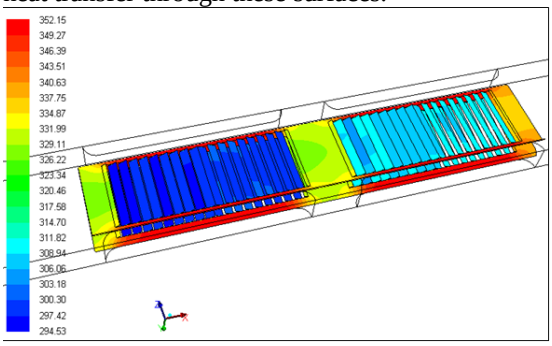

Fig. 18 Air side heat transfer coefficient contour on wall surfaces (Case-06)

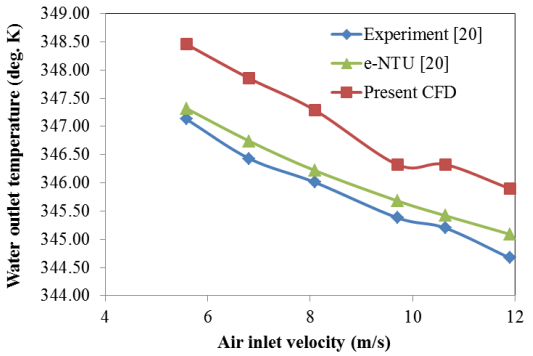

Fig. 19 Effect of air inlet velocity variation on water outlet temperature

Figure 19 shows the effect of air inlet velocity on the water outlet temperature. The results from the present CFD computations are compared with the experimental results of Vaisi *et al.* [16] and the results are found to be in good agreement with the experimental results. The present CFD results slightly over predicted the water outlet temperatures as the present computations did not consider the loss of heat to the ambient by convection and radiation, which is inevitable in the case of experiments.

By using a scale factor of 0.9965, the present CFD predicted water outlet temperature can be brought down to the experimental results. This will help in reducing the number of experimental trials needed and the attention can be focussed on conducting more numerical iterations. With the increase in inlet air velocity, the air flow rate passing through the domain increases and hence the heat carried by the air. This causes more heat transfer from the hot water to the air, making the water outlet temperature drops.

Figure 20 shows the influence of inlet air velocity on the air outlet temperature. Present CFD results shows lower values of air outlet temperature as against the experimental values. This indicates that the predicted heat transfer coefficient is lesser than the actual experimental values due to the fact that the energy from hot water in the form of convective and radiative heat transfer is not captured in the present simulations. When included, the air outlet temperature could have increased.

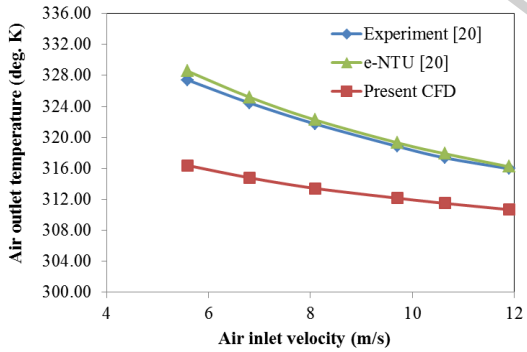

Fig. 20 Effect of air inlet velocity variation on air outlet temperature

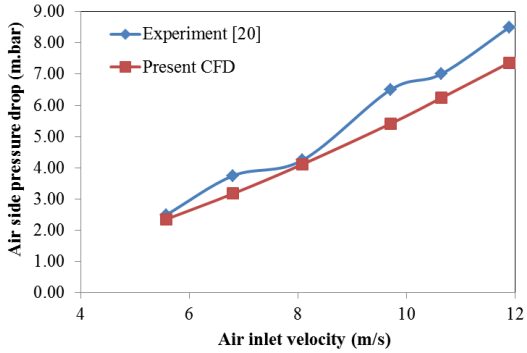

Fig. 21 Effect of air inlet velocity variation on air side pressure drop

Figure 21 shows the effect of air inlet velocity on the air side pressure drop. The values from the present computations are in good agreement with the values from experiments. Experimental values of Vaisi *et al* [16] showed a small fluctuation in air side pressure drop at air inlet velocity closet to 8m/s. This could be due to some instrument glitch. These results confirm again that the computational methodology presently adopted is validated

Effect of Water Flow Rate (Cases 11-15)

To study the influence of water flow rate on the channel performance, different water flow rates in the range of 80-130LPM in steps of 10LPM were tested numerically. 120LPM being the base line case, which is reported in the validation study itself, results from another flow rate of 80 LPM, the lowest water flow rate (Case-11) is reported here.

Figure 22 shows the air side heat transfer coefficient on the wall surfaces of the fins, louvers and water tubes.

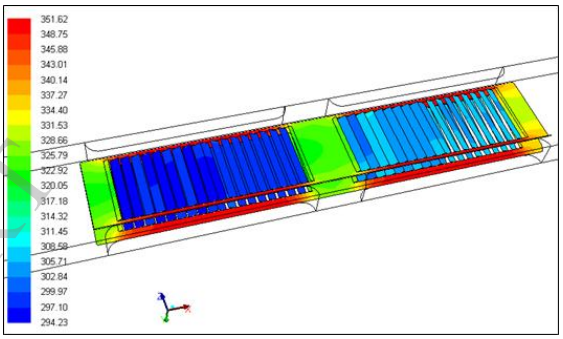

Fig. 22 Air side heat transfer coefficient contour on wall surfaces (Case-11)

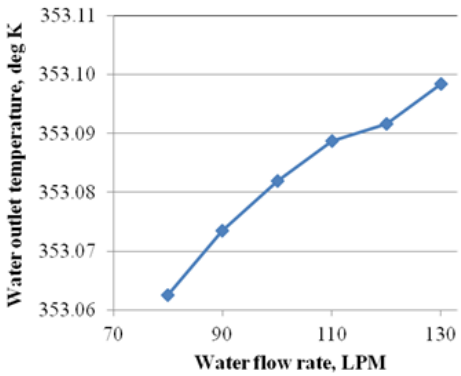

Fig. 23 Effect of water flow rate variation on water outlet temperature.

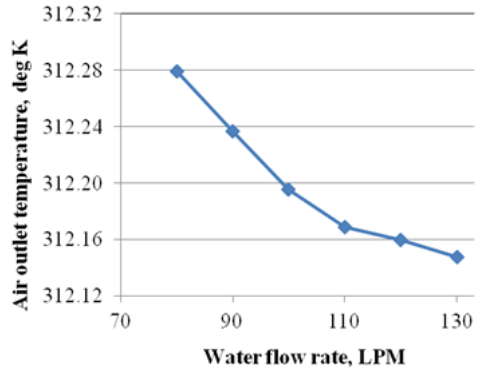

Fig. 24 Effect of water flow rate variation on air outlet temperature.

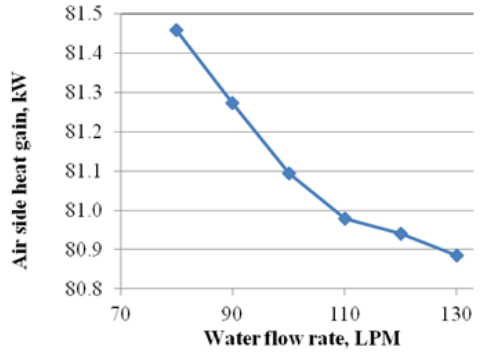

Fig. 25 Effect of water flow rate variation on air side heat gain

Figures 23 and 24 show the effect of water flow rate on water and air outlet temperatures respectively. With increase in water flow rate, water outlet temperature increases and air outlet temperature decreases. This may be attributed to the lesser residence time for water to transfer heat to the air. Figure 25 shows the influence of water flow rate on air side heat gain, which shows a decreasing trend. This is in-line with the air outlet temperature trend for the given air flow rate.

Effect of Fin, Louver Thickness (Cases 16-19)

The fin and louver thickness plays a major role in heat transfer as conduction across the thickness of these surfaces determines the total heat transfer. Hence two more thicknesses for the fin and louver surfaces viz., 0.04mm and 0.12mm were tested numerically.

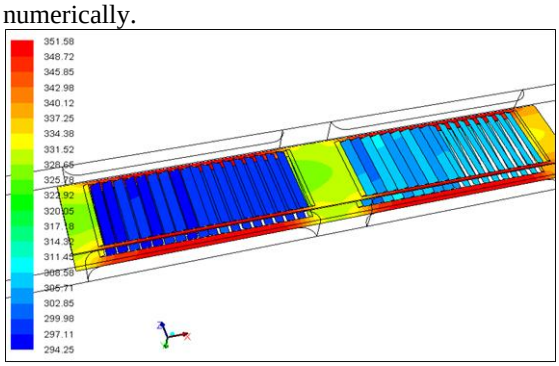

Fig. 26 Air side heat transfer coefficient contour on wall surfaces (case-17)

Figure 26 shows the air side heat transfer coefficient on the wall surfaces of the fins, louvers and water tubes.

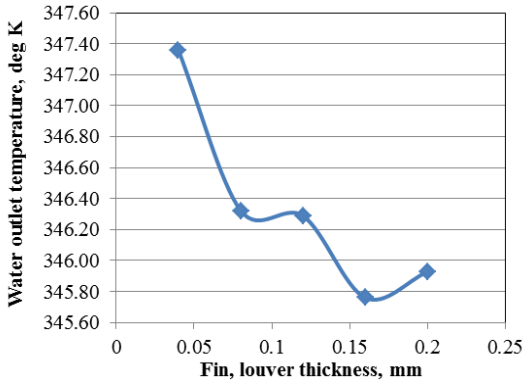

Fig. 27 Effect of fin and louver thickness variation on water outlet temperature

Fig. 27 shows the effect of fin and louver thickness variation on the water outlet temperature, which indicates that there is no effect of thickness on this parameter.

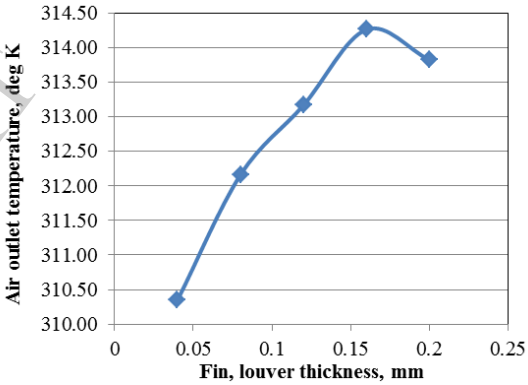

Fig. 28 Effect of fin and louver thickness variation on air outlet temperature

Air outlet temperature increases with increase in fin and louver thickness as shown in Fig. 28. Figure 29 shows that the air side heat gain increases with increase in fin and louver thickness. Increase of louver, fin thickness initially increased the heat transfer and beyond 0.16mm thickness, the net heat transfer decreases. This could be due to the increase in conductive thermal resistance.

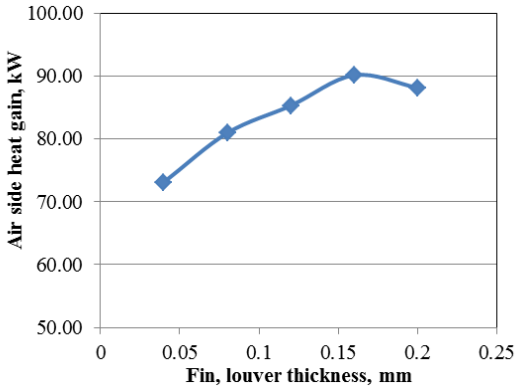

Fig. 29 Effect of fin and louver thickness variation on air side heat gain

Conclusions

Numerical analysis was carried out on a compact heat exchanger domain identified from literature. Validation of the present computational methodology was performed to vindicate it and further analysis was extended to include flow and geometry parameters. The following are the conclusions identified from the present numerical analysis.

1. The present computational methodology is validated by comparing the results from the present CFD analysis with the experimental results.
2. The results from the computations are found to be in good agreement with that of the experiments.
3. Increasing the louver pitch helped in reducing the pumping power requirements with increase in net heat transfer coefficient. This will help in increasing the power output per unit mass of the radiator. Hence it is recommended to increase the louver spacing for the geometry under consideration.
4. Increasing air flow rate showed significant increase in heat transfer. Even though increased air flow could be a suggestion, it incurs an additional pumping power. Hence it is suggested to choose the optimal flow rate in combination with the optimal louver spacing.
5. Lower water flow rate showed higher heat transfer from the water side to the tube side. An optimal number can help increasing the performance better.
6. Increased louver, fin thickness helped in increasing the overall heat transfer. However, an optimal louver and fin thickness should be identified for getting the maximum heat transfer benefit.

As an extension of this work, the following are suggested to continue as a future work. Optimize louver pitch and air flow rate in combination to find the right combination of these parameters. Studying the louver angle influence by considering other louver angles like 15, 20 and 30 degrees to find optimal louver angle could be carried out. Tube pitch and fin pitch effect can be studied to find the optimal values for these parameters.

References

[1] R. Saidur, K.Y. Leong and H.A. Mohammad, A Review on Applications and Challenges of Nanofluids. Renewable and Sustainable Energy Reviews, 15, 3 (2011), 1646–1668.

[2] Pelaez, R.B., Ortega, J.C., Cejudo-Lopez, J.M., A three-dimensional numerical study and comparison between the air side model and the air/water side model of a plain fin and tube heat exchanger, Applied Thermal Engineering, 30 (2010), pp.1608-1615.

[3] Sahin, H.M., Dal, A.R., Baysal, E., 3-D Numerical study on correlation between variable inclined fin angles and thermal behavior in plate fin-tube heat exchanger, Applied Thermal Engineering, 27 (2007), pp.1806-1816.

[4] Wen, M.Y. Ho, C.Y., Heat transfer enhancement in fin and tube heat exchanger with improved fin design, Applied Thermal Engineering, 29(2009), pp.1050-1057.

[5] Yan, W.M., Sheen, P.J., Heat transfer and friction characteristics of fin and tube heat exchangers, International Journal of Heat and Mass Transfer, 43 (2000), pp.1651-1659.

[6] Wolf, I., Frankovic, B., Vilicic, I., A numerical and experimental analysis of neat transfer in a wavy fin and tube heat exchanger, Energy and the Environment (2006) pp.91-101.

[7] Tang, L.H., Zeng, M., Wang, Q.W., Experimental and numerical investigation on air side performance of fin and tube heat exchangers with various fin patterns, Experimental Thermal and Fluid science, 33(2009), pp.818-827.

[8] Wang, C.C., Lo, J, Lin, Y.T. Wei, C.S., Flow visualization of annular and delta winlet vortex generators in fin and tube heat exchanger application, International Journal of Heat and Mass Transfer, 45, (2002), pp.3803-3815.

[9] Fiebig, M., Valencia, A., Mitra, N.K.., Local heat transfer and flow losses in fin and tube heat exchangers with vortex generators: A comparison of round and flat tubes, Experimental Thermal and Fluid Science, 8(1994), pp.35-45.

[10] Leu, J.S., Wu, Y.H., Jang, J.Y., Heat transfer and fluid flow analysis in plate-fin and tube heat exchangers with a pair of block shape vortex generators, International Journal of Heat and Mass Transfer, 47 (2004), pp. 4327-4338.

[11] Leu, J.S., Liu, M.S., A numerical investigation of louvered fin and tube heat exchangers having circular and oval tube configurations, International Journal of Heat and Mass Transfer, 44 (2001), pp. 4235-4243.
[12] Joen, C.T *et. al.*, Interaction between mean flow and thermo-hydraulic behaviour in inclined louver fins, International Journal of Heat and Mass Transfer, 54, (2011), pp.826-837.
[13] Zhang, X., Tafti, D.K., Flow efficiency in multi-louvered fins, International Journal of Heat and Mass Transfer, 46, (2003), pp.1737-1750.
[14] Li, W., Wang, X., Heat transfer and pressure drop correlations for compact heat exchangers with multi-region louver fins, International Journal of Heat and Mass Transfer, 53 (2010), pp.2955-296.
[15] Wang, C.C., Lee, C.J., Chang, C.T., Lin, S.P., Heat transfer and friction correlation for compact louvered fin and tube heat exchangers, International Journal of Heat and Mass Transfer, 42 (1999), pp.1945-1956.
[16] A.Vaisi, M. Esmaeilpour and H. Taheria, Experimental investigation of geometry effects on the performance of a compact louvered heat exchanger. Applied Thermal Engineering 31 (2011) 3337-3346.
[17] An Introduction to CFD - the FVM, 1995, Longman Scientific and Technical, England.
[18] B. E. Launder and D. B. Spalding, Mathematical Models of Turbulence, Academic Press (1972).
[19] Shih, T.-H., Liou, W.W., Shabbir, A., Yang, Z., and Zhu, J., 1995, A New k-e Eddy-Viscosity Model for High Reynolds Number Turbulent Flows - Model Development and Validation. Computers Fluids, 24(3):227-238.
[20] Wilcox, D. C., 1998, Turbulence Modeling for CFD, DCW Industries Inc., La Canada, California.